Discrete stochastic model of point defect-dislocation interaction for simulating dislocation climb

Cameron McElfresh [a], Yinan Cui [b,d], Sergei L. Dudarev [c], Giacomo Po [e], Jaime Marian [a,d,*]

[a] *Department of Materials Science and Engineering, University of California, Los Angeles, CA, 90095, USA*
[b] *Applied Mechanics Laboratory, School of Aerospace Engineering, Tsinghua University, Beijing, 100084, China*
[c] *United Kingdom Atomic Energy Authority, Culham Science Centre, Abingdon, OX14 3DB, UK*
[d] *Department of Mechanical and Aerospace Engineering, University of California, Los Angeles, CA, 90095, USA*
[e] *Mechanical and Aerospace Engineering Department, University of Miami, Coral Gables, FL, 33146, USA*

ARTICLE INFO

ABSTRACT

Dislocation climb is an important high temperature process in metals plasticity, responsible for the phenomena such as creep, swelling, or hardening. Climb is defined by the ability of dislocations to leave their original glide plane by interacting with point defects. As such, dislocation climb is controlled by point defect diffusion/absorption/emission, all of which involve thermal activation. The existing thermodynamically consistent models for climb are generally formulated in a continuum framework, through the definition of effective defect fluxes and climb propensities in response to thermodynamic driving forces. However, the point-wise discrete nature of vacancies (and/or self-interstitials) confers a highly discrete nature to the climb dynamics, which is also strongly affected by elastic forces. The combination of discreteness, thermal activation, and elasticity makes this process too challenging for direct atomistic methods such as molecular dynamics. Here we develop a kinetic Monte Carlo model that captures vacancy generation and transport kinetics acting in conjuction with the evolving elastic fields provided by discrete dislocation dynamics simulations. The two models are coupled via the applied stresses and stress gradients generated by dislocation structures at vacancy locations. Our simulations reveal two surprising results. First that climb is dominated by vacancy emission even when the background vacancy concentration is much higher than the equilibrium one. And, second, that climb velocities might be much faster than otherwise believed when one uses the classical theories of climb. These effects are due to the locality of vacancy-dislocation processes, which are not captured in classical treatments that assume smooth vacancy fluxes and homogeneous concentrations. We apply the method to study elementary climb processes in body-centered cubic iron and furnish climb mobility functions to be used in parametric dislocation dynamics and/or crystal plasticity simulations. We apply the technique to study non-conservative plastic bypass of spherical precipitates by edge dislocations and point out the differences between our discrete approach and existing continuum formulations.

* Corresponding author. Department of Materials Science and Engineering, University of California, Los Angeles, CA, 90095, USA.
E-mail address: jmarian@ucla.edu (J. Marian).

1. Introduction

Non-conservative dislocation motion is responsible for important processes in plasticity such as climb, jog-dragging, the closing of cross-kinks, among others, with significant implications for mechanical behavior such as e.g. hardening, creep, dynamic strain aging, or swelling in irradiated materials (Weertman, 1955; Messerschmidt, 1970; Mohamed and Langdon, 1974; Strunk and Frydman, 1975; Mansur, 1979; Hong, 1986; Louchet and Viguier, 2000; Marian, Cai and Bulatov, 2004; Stukowski et al., 2015). Generally speaking, non-conservative motion refers to a point defect-assisted process that allows a dislocation segment to leave its glide plane in the direction of its normal. This normal n is uniquely defined as $n \equiv s \times t$, where $s = b/b$ is the slip direction (b is the Burgers vector and $b = \|b\|$) and t is the local tangent vector defining the local direction of the dislocation line. The necessity of point defect intervention makes processes like climb only feasible either at high temperatures (via vacancies, when their thermal concentration and/or emission rate is sufficiently high), or under far-from-equilibrium conditions as for example when irradiation is involved (Bullough and Hayns, 1975; Mansur, 1979; Rovelli et al., 2017, 2018).

For a dislocation segment to undergo climb, net defect fluxes must establish themselves, implying the presence of local sub or supersaturation. In its most common manifestation, stress fields produce the concentration gradients that lead to non-conservative dislocation climb. Also, dislocations are strong sinks in situations of supersaturated vacancy concentrations (Bullough and Hayns, 1975; Bullough and Quigley, 1981; Stoller, 1990), so that climb can be regarded as a process that acts to reconstitute thermal equilibrium. Due to its non-conservative nature, dislocation climb is a process by which dislocations can produce volumetric and dimensional changes in addition to slip.

Due to its intrinsically atomic nature, studies of climb processes have been attempted by direct molecular dynamics (MD) simulations (e.g. Wang et al. (2009)) and/or lattice-based kinetic Monte Carlo (kMC) (Kabir et al., 2010; Sivak et al., 2011). However, apart from exceptionally rare situations, vacancy transport at the lattice level is far too slow to be accessible to atomistic simulations in a statistically meaningful manner. Instead, mean-field continuum models, based on the adiabatic approximation, have been the preferred choice in terms of theoretical implementations of climb processes in crystal plasticity and/or dislocation dynamics models. Within these, the more popular approach has been to superimpose a chemical force on the standard elastic forces due to external and internal stresses (Lothe and Hirth, 1967; Turunen, 1976; Raabe, 1998; Mordehai et al., 2008; Bakó et al., 2011; Gu et al., 2015; Thompson et al., 2018). This force is obtained by matching the work done when a dislocation segment climbs a certain distance with the free energy required to create the vacancies needed to climb that same distance. An alternative approach is to formulate the climb velocity directly from the vacancy transport equations in the presence of dislocations (Fischer and Svoboda, 2011; Keralavarma et al., 2012; Davoudi et al., 2012; Rajaguru and Keralavarma, 2018; Liu et al., 2019).

Implementations of climb in discrete dislocation dynamics (DDD) simulations by way of suitable modifications to dislocation mobilities (Cai and Bulatov, 2004; Arsenlis et al., 2007) have been applied successfully in many scenarios (Bakó et al., 2011; Davoudi et al., 2012; Keralavarma et al., 2012; Haghighat et al., 2013; Záležák et al., 2017; Liu et al., 2019). These approaches are all formulated at the continuum level, which – while thermodynamically consistent and numerically efficient – disregard local fluctuations in stress and defect concentrations. These fluctuations are especially important under heterogeneous conditions, when spatially-complex dislocation structures and/or defect distributions (e.g. as during irradiation) exist. Since vacancies are discrete particles, they are highly sensitive to these local variations of stress and presence of other defects. Thus, understanding how they evolve, taking into account such fluctuations, and studying how sensitive climb processes are to spatial heterogeneities is of relevance in many cases. The objective of this work is to superimpose a kMC module tasked with simulating vacancy diffusion onto a microstructural simulator based on DDD, tasked with updating dislocation structure morphology and stress fields. As such, the kinetic module and the DDD simulator are coupled together by the underlying stress fields in the simulation volume. Vacancy transport is modeled using a drift-diffusion equation with the drift velocity depending on the spatial stress state in the system. One of our objectives is to determine effective climb rates as a function of temperature and vacancy concentration for isolated dislocations, as well as to study the effects on arbitrary dislocation structures of a vacancy supersaturation.

The paper is organized as follows. First, we provide a formal theoretical framework for the kinetic transport model. This is followed by a description of the numerical implementation and modifications to the DDD simulator. Then, verification benchmarks are presented to check the validity of the approach at the local dislocation level, followed by calculations of climb rates in well-controlled conditions. We also discuss the effect of varying parametric parameters on computational cost. Next, we show results demonstrating bypass of a spherical precipitate by an edge dislocation. We finalize the paper with a discussion of the results and the conclusions.

2. Underlying theory

2.1. Kinetic model for point defect diffusion

According to transition state theory (Vineyard, 1957; Laidler and King, 1983), the diffusion coefficient for vacancies hopping in an isotropic medium follows an Arrhenius expression of the following type:

$$D(T) = zfb^2\nu(T) \tag{1}$$

where z is the coordination number of the lattice in question ($z = 8$ for bcc crystals), f is a correlation factor, b is the crystallographic jump distance ($b = a_0\sqrt{3}/2$ for bcc crystals, a_0 is the lattice parameter) and $\nu(T)$ is the temperature dependent jump frequency of the

form

$$\nu(T) = \nu_0 \exp\left(-\frac{\Delta H_m}{kT}\right) \tag{2}$$

where ν_0 is an attempt frequency, k is Boltzmann's constant, and ΔH_m is the vacancy migration enthalpy. In the low-stress limit, ΔH_m depends on stress $\boldsymbol{\sigma}$ via a mechanical work coupling:

$$\Delta H_m(\boldsymbol{\sigma}) = \Delta E_m^0 - \boldsymbol{\sigma} : \boldsymbol{\Omega}_{\mathrm{act}}$$

where ΔE_m^0 is the migration energy of a vacancy in a solid subjected to no stress, and $\boldsymbol{\Omega}_{\mathrm{act}}$ is the activation volume tensor defined as the difference between the relaxation volume tensors at the saddle point and at an equilibrium position. Parameters ν_0, ΔE_m^0, and $\boldsymbol{\Omega}_{\mathrm{act}}$ are routinely computed using first principles methods (Ma and Dudarev, 2019 a).

Another, and often more significant, effect of stress on the diffusion of defects results from the fact that the enthalpy of formation of a defect at an equilibrium position in the lattice depends on the local stress through:

$$H_f(\boldsymbol{\sigma}) = E_f^0 - \boldsymbol{\sigma} : \boldsymbol{\Omega}_f \tag{3}$$

where E_f^0 is the defect formation energy and $\boldsymbol{\Omega}_f$ is the formation volume tensor (Ma and Dudarev, 2019 a,b). It must be noted, however, that in most cases it is the relaxation, and not the formation, volume of a defect that enters the equations of elasticity, since it is the relaxation of the lattice around a defect that determines its elastic interaction with other defects and dislocations. As such, the relaxation volume tensor provides a tensorial measure of global deformation of the material due to the presence of a defect in it (Puchala et al., 2008).

The relaxation and formation volume tensors, $\boldsymbol{\Omega}$ and $\boldsymbol{\Omega}_f$, are related to one another via $\boldsymbol{\Omega}_f = \pm \frac{1}{3}\Omega_a \boldsymbol{I} + \boldsymbol{\Omega}$, where Ω_a is the atomic volume, and the sign of Ω_a depends on the nature of the defect, vacancy ($+$) or self-interstitial ($-$) (Kraftmakher, 1998). For vacancies, the first term in the above relation is positive, since in order to form an individual vacancy in the bulk of the crystal, it is necessary to deposit an atom onto its surface, hence increasing the total volume of the material by one atomic volume Ω_a. Conversely, the formation of a self-interstitial atom involves punching a surface atom into the bulk of the material, hence reducing the apparent total volume by Ω_a.[1] The second term, $\boldsymbol{\Omega}$, entering the formula for $\boldsymbol{\Omega}_f$, is the relaxation volume tensor (Ma and Dudarev, 2019 a,b), describing the lattice relaxation effects. Elements of the relaxation volume tensor of a point defect can be readily evaluated using first-principles calculations (Ma and Dudarev, 2019 a,b).

Note that in the context of studies of radiation damage, the *formation* volumes of defects rarely enter the equations for the experimentally observed quantities. That is because, under irradiation, vacancies and self-interstitial defects are formed in pairs, and this results in the cancellation of terms $\pm\frac{1}{3}\Omega_a \boldsymbol{I}$ in the definition (Ma and Dudarev, 2019 a) of the formation volume tensor $\boldsymbol{\Omega}_f$ above. Also, one should recognize the difference between the volumetric swelling of a material, which is a quantity given by the sum of formation volumes of all the defects, and lattice strain, measured for example by X-ray diffraction. Lattice strain is a measure of relaxation of the lattice, and it therefore depends on the *relaxation* volumes of defects, as illustrated for example by the observed negative lattice strain resulting from the accumulation of vacancies in metals (Hertz et al., 1973).

The trace of the relaxation volume tensor $\mathrm{Tr}(\boldsymbol{\Omega}) = \Omega_{kk} = \Omega_{11} + \Omega_{22} + \Omega_{33}$ gives the total relaxation volume of a defect Ω_{rel}, which, depending on its sign (negative or positive), provides a measure of the total elastic contraction or expansion of the lattice due to the presence of the defect in the material (Dudarev et al., 2018). For a vacancy, the relaxation volume tensor is isotropic (Dudarev et al., 2018), namely $\Omega_{ij} = \frac{1}{3}\delta_{ij}\Omega_{\mathrm{rel}}$, where δ_{ij} is Kronecker's delta. Since the trace of the identity tensor $\mathrm{Tr}(\boldsymbol{I}) = \delta_{kk} = \delta_{11} + \delta_{22} + \delta_{33} = 3$, we find $\mathrm{Tr}(\boldsymbol{\Omega}) = \frac{1}{3}\Omega_{\mathrm{rel}}\mathrm{Tr}(\boldsymbol{I}) = \Omega_{\mathrm{rel}}$. In terms of atomic volume, we can express the relaxation volume tensor as (Ma and Dudarev, 2019 a,b):

$$\boldsymbol{\Omega} = \Omega_a \boldsymbol{\varepsilon}_v \tag{4}$$

where $\boldsymbol{\varepsilon}_v$ is a diagonal strain tensor with identical components $\varepsilon_v = (\boldsymbol{\varepsilon}_v)_{11} = (\boldsymbol{\varepsilon}_v)_{22} = (\boldsymbol{\varepsilon}_v)_{33}$ equal to:

$$\varepsilon_v = \frac{\Omega_{\mathrm{rel}}}{3\Omega_a} = \frac{\theta_v}{3}$$

with θ_v being the relative local lattice contraction around a vacancy (typically around -20% (Ma and Dudarev, 2019 a,b)). With this, assuming that the relaxation volume of a defect is isotropic, eq. (3) becomes:

$$H_f = E_f^0 - \frac{1}{3}\sigma_{ij}\delta_{ij}(\Omega_{\mathrm{rel}} \pm \Omega_a) = E_f^0 - \frac{1}{3}\sigma_{jj}(\Omega_{\mathrm{rel}} \pm \Omega_a) = E_f^0 + p(\Omega_{\mathrm{rel}} \pm \Omega_a) \tag{5}$$

where, as above, '$+$' refers to vacancies and '$-$' to self-interstitials, and $p = -\frac{1}{3}\mathrm{Tr}(\boldsymbol{\sigma}) = -\frac{1}{3}\sigma_{kk} = -\frac{1}{3}(\sigma_{11} + \sigma_{22} + \sigma_{33})$ is the hydrostatic pressure (Landau and Lifshits, 1970). Note that in the above equations we use the Einstein convention where repeated indeces imply summation. The energy of a defect at an equilibrium position in the lattice depends on the stress as follows (Heald and Speight, 1975;

---

[1] See for example Fig. 14.10 from Hirth and Lothe (1992).

Bullough and Newman, 1970):

$$E = E^0 - \frac{1}{3}\sigma_{ij}\delta_{ij}\Omega_{\text{rel}} = E^0 - \frac{1}{3}\sigma_{kk}\Omega_{\text{rel}} = E^0 + p\Omega_{\text{rel}}. \tag{6}$$

In the approximation where both the relaxation and activation volume tensors of a defect are assumed to be isotropic, the diffusion tensor is also isotropic (Bullough and Newman, 1970; Dederichs and Schroeder, 1978). This justifies the drift-diffusion equation approach developed below.

2.2. The drift-diffusion equation

Vacancy transport is governed by the so-called the drift-diffusion (or advection-diffusion) equation:

$$\frac{\partial C}{\partial t} = D\nabla^2 C - u \cdot \nabla C \tag{7}$$

where C is the defect concentration, u is the average drift velocity (a three-dimensional vector), ∇ is the gradient operator, D is the diffusion coefficient, and ∇^2 is the Laplacian. The first term on the right-hand side of eq. (7) represents drift due to the bias in the probability of moving in a preferred direction and the second term describes ordinary isotropic three-dimensional diffusion. For walkers centered at the origin, the above equation has the following solution in one dimension (Codling et al., 2008; Blaj et al., 2017)

$$C(x,t) = \frac{1}{(4\pi Dt)^{1/2}}\exp\left\{-\frac{(x-ut)^2}{4Dt}\right\} \tag{8}$$

where t is the time and x is the position vector. Useful time-dependent statistics of this process are the mean location $m(X_t)$ (first moment of the $C(x,t)$ distribution) and the mean squared displacement (MSD) $m(R_t^2)$ (second moment, with $R_t = |X_t|$), defined as:

$$m(X_t) = \int x C(x,t)dx \tag{9}$$

$$m(R_t^2) = \int |x|^2 C(x,t)dx \tag{10}$$

The solutions to the above integrals are $m(X_t) = ut$ and:

$$m(R_t^2) = u^2 t^2 + 6Dt$$

That is, the effect of the drift compared to a simple random walk process is to shift the center of the Gaussian distribution from $x = 0$ to $x = ut$ and to make the MSD depend quadratically on time (for long times) instead of linearly.

The drift term can be obtained by mapping eq. (7) to the general form of the diffusion equation for isotropic cubic crystals (Dederichs and Schroeder, 1978):

$$\frac{\partial C(x,t)}{\partial t} = \nabla \cdot \left[D\left(\nabla C(x,t) + \frac{C(x,t)}{kT}\nabla E(x)\right)\right] \tag{11}$$

where the energy gradient term reflects the variation of the energy of defects at equilibrium lattice sites. Equation (11) is encountered in the treatment of diffusion of particles in a potential energy field $E(x)$, where the right-hand side of the equation equals the divergence of the defect flux. Comparing the second terms in the r.h.s. of eqs. (7) and (11) gives the expression for the drift velocity u is:

$$u = -\frac{D}{kT}\nabla E(x) \tag{12}$$

Inserting eq. (6) into the above expression results in the drift velocity being proportional to the gradient of the pressure:

$$u = \frac{D\Omega_{\text{rel}}}{3kT}\nabla\text{Tr}(\boldsymbol{\sigma}(x)) = -\frac{D\Omega_{\text{rel}}}{kT}\nabla p(x) \tag{13}$$

In the above expression, we have neglected the variation of the diffusion coefficient with spatial coordinates. This variation is associated with the change of shape of the strain field of a vacancy during its transition across a saddle point (Ma and Dudarev, 2019 a), and it adds an extra term, quadratic in stress, to the right-hand side of eq. (13). We have also neglected the dependence of the relaxation volume on stress, and retained only the term linear in elastic field (see Leibfried and Breuer (1978)). With this, equation (13) can be expressed in explicit Cartesian form as:

$$u_i = \frac{D\Omega_{\text{rel}}}{3kT}\frac{\partial\sigma_{kk}}{\partial x_i}, \tag{14}$$

where $\sigma_{kk} \equiv \text{Tr}(\boldsymbol{\sigma})$.

2.3. Vacancy production/elimination mechanisms

2.3.1. Vacancy absorption

Once a vacancy or a number of vacancies N_i reaches a given dislocation segment i of length ℓ_i, the following volume balance can be written:

$$N_i \Omega_a = \ell_i h_i (t_i \times \boldsymbol{b}_i) \cdot \boldsymbol{n}_i$$

where h_i is the climb distance along the normal direction $\boldsymbol{n}_i$, $\boldsymbol{b}_i$ and $b_i = |\boldsymbol{b}|$ are the Burgers vector and its modulus, and t_i is the segment direction. This results in a climb jump of magnitude:

$$h_i = \frac{N_i \Omega_a b_i}{\ell_i |t_i \times \boldsymbol{b}_i|^2} \tag{15}$$

where we have used that $\boldsymbol{n} = (t \times \boldsymbol{b})/b$. Note that h_i is undefined for screw dislocations, as is commonly the case in this type of models (Turunen, 1976; Bakó et al., 2011).

2.3.2. Thermal vacancy emission

After Friedel (Friedel and Yoshida, 1975), the rate of emission of vacancies from dislocations can be written as:

$$\dot{C} = q\nu(T)\left(1 - \frac{C}{C_0}\right) \tag{16}$$

where q is a geometric factor, $\nu(T)$ is the vacancy jump rate (refer to eq (2)), and $C_0 = \exp\left(-\frac{H_f}{kT}\right)$ is the equilibrium vacancy concentration (H_f is the vacancy formation enthalpy, eq. (5)).

Expression (16) is nonlocal, i.e., it is enforced in a global sense (as defined by C_0). However, vacancy emission from a dislocation segment is highly local in that it is strongly influenced by the local stress and vacancy concentration. Consequently, the above equation can be adapted to give the local emission from a given dislocation segment of length ℓ surrounded by a number of vacancies N in a volume around the segment. Further, here we take the approach that the emission rate is zero for purely screw segments and maximum for pure edge segments. With this, we can write:

$$\dot{N}_i = \left(\frac{2\pi\ell_i}{b_i}\left(1 - \frac{t_i \cdot \boldsymbol{b}_i}{b_i}\right)\right)\nu(T)\left(1 - \frac{N_i}{\rho_a V_i \exp\left(-\frac{H_f}{kT}\right)}\right) \tag{17}$$

where N_i is the number of vacancies contained in a volume $V_i = \pi R^2 \ell_i$ around dislocation segment i. The stress σ in this volume is taken to be the local stress (from sources other than the self-stress) at the dislocation segment's location, r_i. In principle, R is arbitrary but it should be sufficiently small for this approximation to be valid. Note that in most cases, this will result in zero vacancies in this volume, meaning that the rate of insertion will generally be positive.[2] To avoid repeated emission/reabsorption cycles, we place the emitted vacancies at a random location within the simulation box while displacing the dislocation segment along the negative sense of $\boldsymbol{n}_i$ by an amount consistent with the emitted volume of vacancies (eq. (15)).

Instead of eq. (16), a more consistent expression of the vacancy emission rate needed to maintain a global vacancy concentration is obtained by integrating eq. (17) over the entire simulation volume V[3]:

$$\dot{C}_v = \frac{2\pi V \rho_d}{b}\nu(T)\left(1 - \frac{C_v}{\exp\left(-\frac{H_f(\sigma_{\text{ext}})}{kT}\right)}\right) \tag{18}$$

where ρ_d is the total dislocation density and C_v is the global vacancy concentration. Once a vacancy is emitted using this expression a random segment is selected and displaced by one climb distance h. Emission-dominated conditions lead to 'downward' climb, i.e. along the direction of the tensile region of the stress field of an edge dislocation, while absorption dominated climb takes place 'upwards', or towards the compressive semi-plane.

---

[2] To introduce a stochastic variability in the insertion rate (accepting cases where the vacancy concentration might be higher than the equilibrium concentration, or rejecting cases where the vacancy concentration might be lower than the equilibrium concentration), the second '1' in eq. (17) is replaced with a Gaussian defined by $N(1, kT/E_f^0)$.

[3] Summation of all segments over V yields: $\sum_i \ell_i = \rho_d V$.

2.4. Connection to elasticity and climb mobilities

The climb velocity of a given segment v_c^i points along the direction of n_i and is connected to the climb forces as:

$$
\begin{aligned}
v_c^i &= v_c^i \, \boldsymbol{n}_i \\
v_c^i &= M_c \left(f_i^{\text{el}} + f_i^{\text{os}} \right)
\end{aligned}
\tag{19}
$$

where $M_c \equiv M_c(T, p, C_v)$ is a scalar-valued function representing the climb *mobility*, $f_i^{\text{el}} = [(\boldsymbol{\sigma}_i \cdot \boldsymbol{b}_i) \times \boldsymbol{t}_i] \boldsymbol{n}_i$ is the climb contribution of the Peach-Koehler force, while f_i^{os} is the chemical force, often referred to as 'osmotic' force, which in linearized form can be expressed as (Mordehai et al., 2008; Bakó et al., 2011):

$$
f^{\text{os}} = \frac{bkT}{\Omega_a} \left(1 - \frac{C_0}{C_v} \right)
\tag{20}
$$

We will use these expressions to reconcile the results obtained in Section 3.3 with the elastic formulation of DDD.

2.5. Material parameters

We use bcc Fe as our model system in this work. Point defects in iron have been extensively studied experimentally and computationally over the past several decades and a very accurate numerical database exists from which to get the parameters used here (Johnson, 1964; Kim and Buyers, 1978; Söderlind et al., 2000; Domain and Becquart, 2001; Mendelev et al., 2003; Marian et al., 2004; Fu et al., 2005; Souidi et al., 2006; Fu and Willaime, 2008; Ma and Dudarev, 2019 a,b). They are given in Table 1.

3. Results

Next we apply the method described in the previous section to the calculation of climb velocities for edge dislocations in Fe. The solution procedure and the numerical details of the simulations are discussed in depth in A. First we carry out a set of self-consistency verification checks to ensure the correctness of the model, followed by production runs to calculate climb velocities as a function of temperature, pressure, and global vacancy concentration.
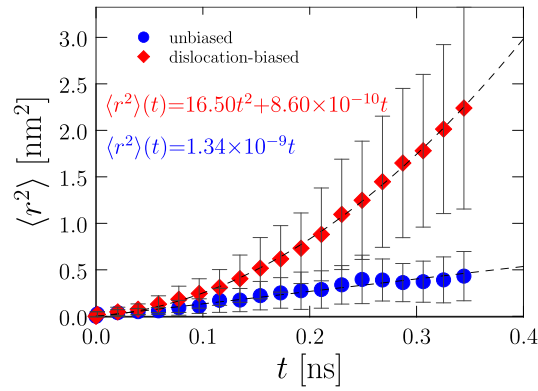
3.1. Self-consistency checks

We begin by testing the evolution of the mean square displacement, $\langle r^2 \rangle$, of vacancies diffusing in an isotropic medium versus vacancies moving in the stress field near the core of an edge dislocation. The results for 200 independent tests (one single vacancy placed at random in a 2D square box) are shown in Fig. 1 with error bars. The evolution of $\langle r^2 \rangle$ in each case displays the expected dependence with time described in Sec. 2.2. The diffusivity used was $1.0 \times 10^{-9} \, \text{m}^2 \cdot \text{s}^{-1}$ ($\sim$300 K in Fe), which correlates well with the values of 8.6×10^{-10} and $1.3 \times 10^{-9} \, \text{m}^2 \cdot \text{s}^{-1}$ displayed in Fig. 1 for biased and unbiased diffusion, respectively.

While tracking the evolution of $\langle r^2 \rangle$ is useful to verify the solution of eq. (7), the mean square displacement is an integrated measure that does not give information about the trajectories of migrating vacancies. To check whether vacancy trajectories are consistent with the drift velocity derived in Sec. 2.2, we plot in Fig. 2 the generic trajectories of vacancies against the backdrop of the (isotropic elastic) stress field of an edge dislocation (shown as a color contour plot) and vector (14). The figure contains results for the σ_{xx} and σ_{yy} components of the stress, as well as for the $\frac{\partial \sigma_{kk}}{\partial x}$ and $\frac{\partial \sigma_{kk}}{\partial y}$ components of (14) (Fig. 2a and b). The vacancy trajectories are clearly seen to follow a biased walk as dictated by the existing stress gradients. The tests performed in Figs. 1 and 2 verify the model of Secs. 2.1 and 2.2 at the local level and gives us confidence to apply it for calculations of dislocation climb in realistic line geometries.

Table 1
Material parameters for bcc Fe employed in this work.

Parameter	Symbol	Value	Units
Boltzmann's constant	k	8.615×10^{-5}	eV $\cdot$K^{-1}
Correlation factor	f	0.78	–
Burgers vector's modulus	b	0.25	nm
Attempt frequency	ν_0	10^{12}	Hz
Vacancy migration energy	ΔE_m^0	0.60	eV
Atomic volume	Ω_a	0.77	b^3
Vacancy relaxation volume	Ω_{rel}	θ_v	Ω_a
Vacancy formation volume	Ω_f	$1 + \theta_v$	Ω_a
Vacancy volumetric strain	θ_v	-0.2	–
Vacancy formation energy	E_f^0	1.7	eV
Capture radius	R	2.0	b

Fig. 1. Time evolution of the mean square displacement, $\langle r^2 \rangle$, of vacancies diffusing in an isotropic medium undergoing an *unbiased* random walk (blue circles) and for vacancies moving in the stress field of an edge dislocation (*biased* random walk, red diamonds). Linear and quadratic least-squares fits are shown for each case. The vacancy diffusivity employed corresponds to a temperature of 300 K. The error bars originate from five independent stochastic runs. (For interpretation of the references to color in this figure legend, the reader is referred to the Web version of this article.)
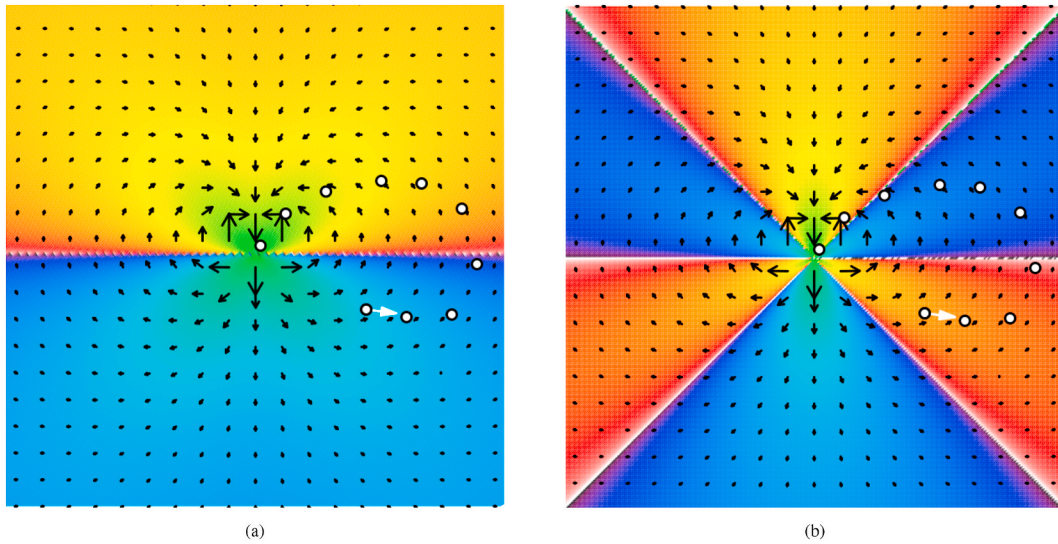

Fig. 2. Stress and stress-gradient maps for an edge dislocation showing: (a) a contour plot of σ_{xx} (red: tensile, blue: compressive, arbitrary units) and the directional field of the $\frac{\partial \sigma_{kk}}{\partial x}$ component of vector (14) (shown with arrows); (b) Corresponding plot for σ_{yy} (red: tensile, blue: compressive, arbitrary units) and $\frac{\partial \sigma_{kk}}{\partial y}$. The trajectories of vacancies initially located at the point marked by the white arrow are highlighted using circles. The vacancy paths are seen to follow the direction of the stress gradient. (For interpretation of the references to color in this figure legend, the reader is referred to the Web version of this article.)

3.2. Dislocation climb calculations

3.2.1. Single dislocation behavior

Next, we systematically study dislocation climb in the ternary parametric space of pressure p, temperature T, and vacancy concentration C_v. To obtain climb velocities, we track the dislocation position normal to the glide plane as a function of time until steady state is reached and a linear relation is established between the two. We then calculate the climb velocity, v_c, as the slope of this linear relationship, as shown in the example in Fig. 3. The graph shows the position of a 100-nm edge dislocation segment obtained from two independent measurements: (i) one according to eq. (15) (labeled 'vacancies absorbed') and (ii) another from the overall dislocation position ('center of mass'). As the figure shows, both approaches are equivalent and result in a climb velocity of 4.62×10^{-4} m·s^{-1}. This value of v_c corresponds to a temperature of $T = 1000$ K, a pressure of $p = -100$ MPa (tensile), with an equilibrium vacancy concentration $C_v \equiv C_0(p, T)$. A direct feature of our model is that h evolves with t in a discrete manner, with clear jumps (e.g. at 15, 26, 35, and 52 ns) correlating with vacancy absorption/emission events. This has a manifestation in the dislocation line morphology. Fig. 4 shows the dislocation structure at the end of the simulation shown in Fig. 3. Vacancies are shown as small cyan spheres. The dislocation
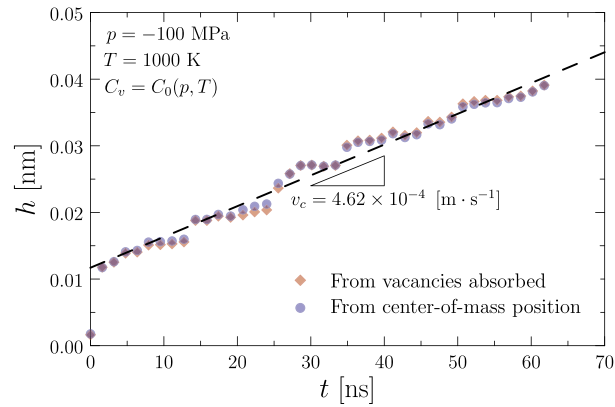
Fig. 3. Dislocation position along the glide plane normal direction h as a function of time t at a temperature of 1000 K and a pressure of -100 MPa (tensile) and equilibrium vacancy concentrations. The graph shows the position obtained from two independent measurements: according to eq. (15) (labeled 'vacancies absorbed') and from the overall dislocation position ('center of mass'). The resulting climb velocity is extracted from a linear fit to the data points in steady state.
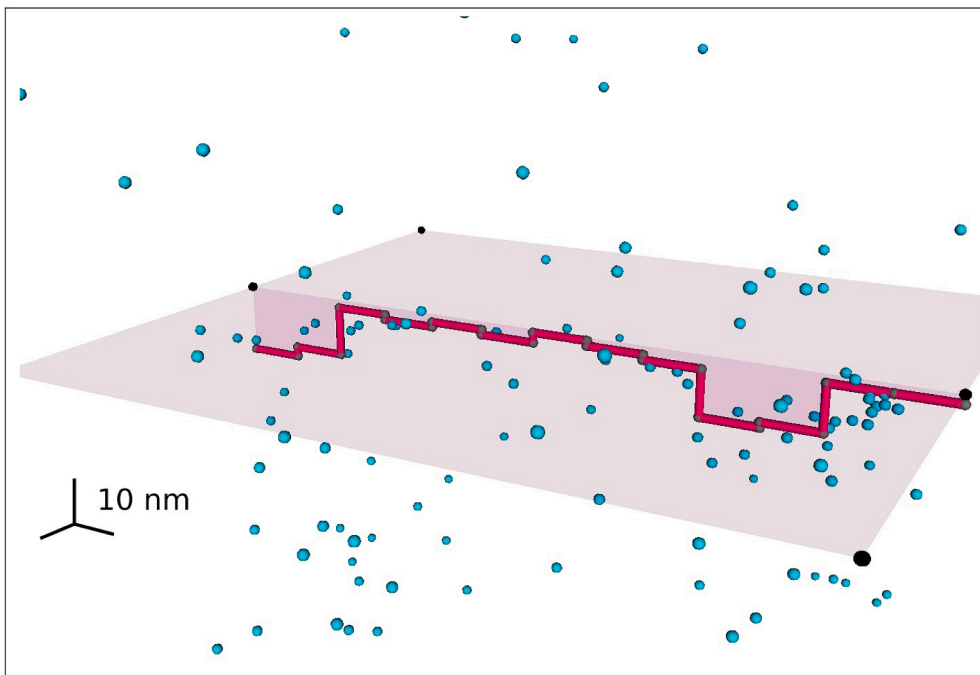

Fig. 4. Dislocation structure after 1 μs at 1000 K and a pressure of -100 MPa with $C_v = C_0(T, p)$. Vacancies are shown as small spheres. The dislocation line displays a number of jogs originating from local vacancy emission (and/or absorption) events. The height of the jogs is commensurate with the Δh jumps displayed in Fig. 3, which are approximately 0.1 Å (single vacancy absorption/emission event). The shaded horizontal plane marks the original glide plane. The shaded region normal to the glide plane marks the slipped climb area. A scale marker for all three Cartesian directions is shown for reference.

line displays a number of jogs consistent with the steps seen in Fig. 3. The shaded horizontal plane marks the original glide plane, while the shaded region normal to the glide plane marks the slipped climb area.

3.2.2. Dislocation climb as a function of temperature, pressure, and vacancy concentration

We repeat the procedure described in the previous to obtain the fundamental climb velocity dependencies as a function of T, p, and C_v. The results are given in Fig. 5, where a sequence of plots is shown with the net climb velocities of edge dislocation segments with lengths ranging between 50 and 500 nm under different combinations of temperature, pressure, and vacancy concentration. The temperature and the pressure set the equilibrium vacancy concentration C_0 according to eq. (16), which at, e.g., -100 MPa and 1000 K (conditions in Fig. 3) is 2.45×10^{-9}. A multiplication factor is then applied to C_0 as to artificially increase the vacancy concentration to
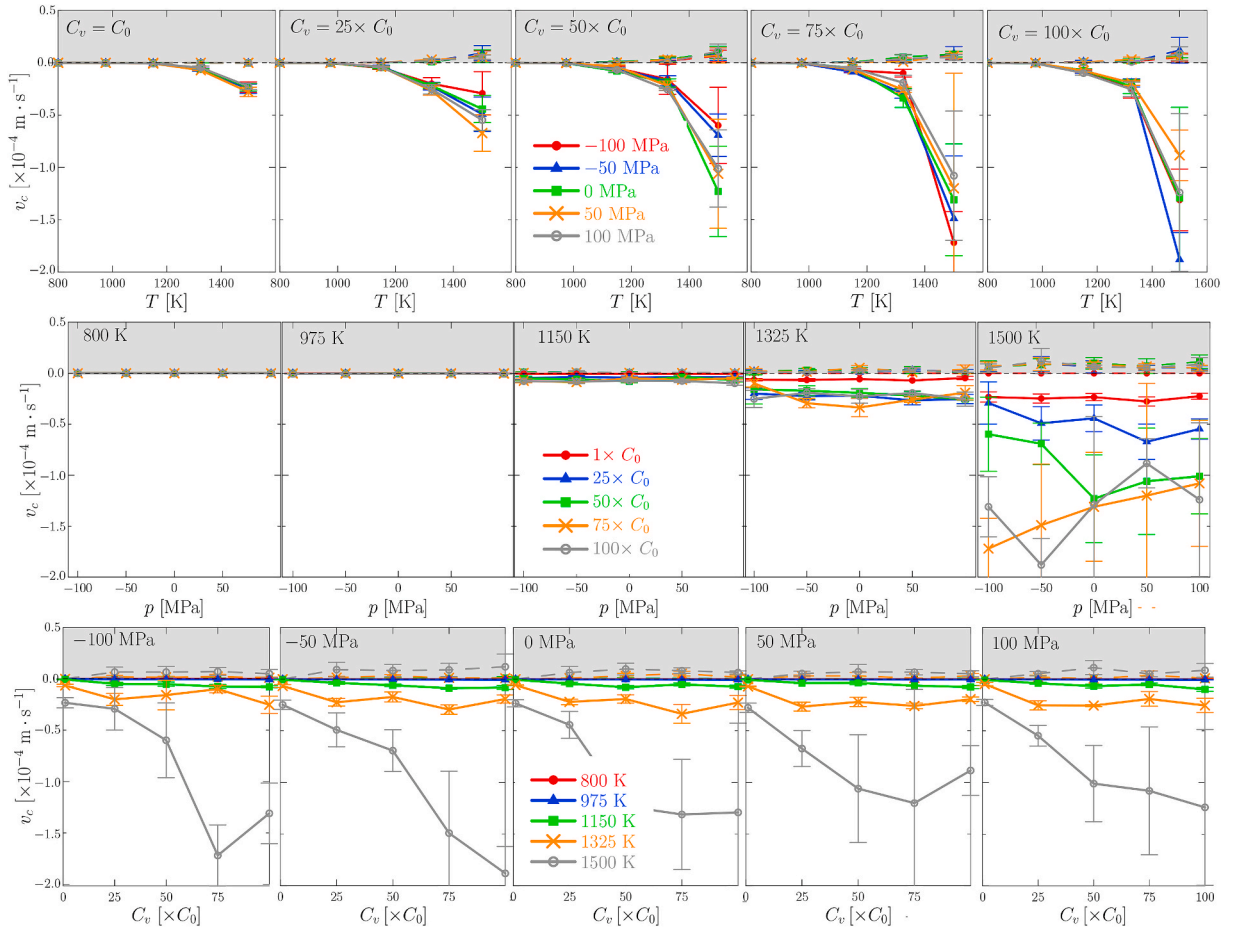
Fig. 5. Sequence of plots showing the net climb velocities of edge dislocation segments with lengths ranging between 50 and 500 nm under different combinations of temperature, pressure, and vacancy concentration. The temperature and the pressure set the equilibrium vacancy concentration C_0 according to eq. (16). Then a multiplication factor is applied to C_0 so as to artificially increase the vacancy concentration to nonequilibrium levels. The average position of the entire dislocation line is then tracked with time and a climb velocity is extracted. Each row of figures shows the climb velocity as a function of a primary variable and two secondary variables. Top row: the primary dependency is on temperature; secondary dependencies are on pressure (colors) and global vacancy concentration (left to right). Middle row: primary dependency on pressure; secondary dependencies on global vacancy concentration (colors) and temperature (left to right). Bottom row: primary dependency on global vacancy concentration; secondary dependencies on temperature (colors) and pressure (left to right). (For interpretation of the references to color in this figure legend, the reader is referred to the Web version of this article.)

nonequilibrium levels to study its effect on v_c. Dislocation climb velocities are calculated as in Fig. 3, with each data point representing the average of five statistically independent simulations. The error bars displayed correspond to the standard deviations for each condition. Each row of figures shows the climb velocity as a function of a primary variable and two secondary variables. In the top row, the primary dependency is on temperature, while secondary dependencies are on pressure (colors) and global vacancy concentration (left to right). In the middle row the primary dependency is on pressure, with secondary dependencies on global vacancy concentration (colors) and temperature (left to right). Finally, the bottom one contains the relationship of the climb velocity with the global vacancy concentration, along with secondary dependencies on temperature (colors) and pressure (left to right). In all curves, dashed lines correspond to climb velocities using eq. (18) for vacancy emission, i.e. when the vacancy concentration is enforced in a 'global' way irrespective of the stress state at each of the dislocation segments. Conversely, continuous lines indicate that the velocities have been calculated under local conditions (with vacancy emission defined by eq. (17)).

Inspection of the results reveals the following general trends:

(i) As indicated earlier, velocities obtained enforcing global vacancy emission tend to be positive (shaded gray region in Fig. 5's plots), while local climb velocities are strongly negative. This points to regimes governed by vacancy absorption and emission, respectively.

(ii) The results are practically insensitive to pressures in the −100-to-100-MPa range.

(iii) The climb velocities have a clear exponential dependence on temperature.

(iv) The total vacancy concentration has an incremental effect on climb velocities, with higher vacancy concentrations resulting in higher values, both positive and negative. In the case of global vacancy emission, a larger C_v results in a higher rate of vacancy absorption and therefore faster positive climb velocities.[4] Enforcing the global vacancy concentration, however, also results in an enhanced emission rate as the differential vacancy concentration around dislocation segments (global minus local) remains positive, keeping eq. (18) active for a longer time, leading to faster negative climb.

To further understand the processes that control the kinetic evolution in the simulations, it is useful to analyze the time step distribution of events. A representative set results is shown in Fig. 6, where we have separated the histogram into a δt-spectrum associated with vacancy diffusion/absorption events (shown in red), and another one corresponding to vacancy emission events (in blue). It can be seen that diffusion/absorption is governed by much faster time scales than vacancy emission. The average of the blue histogram is approximately 3.0 ps, while that of the orange histogram is almost three orders of magnitude higher, ≈ 0.72 ns. These averages are both consistent with eqs. (1), (2) and (17) at the conditions of the simulation.

The large spread in the vacancy emission distribution gives an idea of the wide range of stress spatial variations found in the computational domain. In contrast, vacancy diffusion is defined by a much narrower spectrum. The clear separation of scales between both time distributions results in a numerically-stiff system, which makes it amenable to certain speedup procedures that can increase the computational efficiency (Snyder et al., 2005; Martínez et al., 2008; Núñez and Vlachos, 2015; Savara and Sutton, 2018). In fact, the histogram displayed in the figure points to the causes behind the relatively high computational cost in some of the studied cases. The actual CPU cost of the simulations in Fig. 5 is discussed in A.3 and shown in Fig. A.11.

3.3. Climb mobility functions

We can now use the results from Section 3.2 to parameterize climb mobility functions to be used in *parametric* dislocation dynamics simulations. The climb contribution to the mobility of a dislocation segment i in DDD is given by eq. (19) in Section 2.4. In those equations f^{el} and f^{os} represent two distinct driving forces for dislocation climb:

(i) The existence of non-glide elastic forces, represented by f^{el}, breaks the local vacancy equilibrium at the nodal or segment level, resulting in an imbalance that is resolved by stimulating vacancy diffusion into or out of the dislocation core. As such, these forces can produce climb even in the absence of a *global* vacancy supersaturation. A well-known example of this interaction is climb-induced bypass of precipitates or inclusions blocking dislocations in hardened alloys at high temperatures. While global thermodynamic equilibrium may exist, hydrostatic elastic forces created by the precipitates on dislocations distort local equilibrium facilitating vacancy-assisted climb.

(ii) Complementarily, dislocations can climb in the absence of elastic forces when the global vacancy concentration is far-from-equilibrium e.g. as in quenched metals or irradiation conditions, both of which can produce high vacancy supersaturations. This driving force is represented by f^{os}. Note that, as shown in B, stress gradients confer a mechanical bias to the osmotic force that is not captured in standard theories of dislocation climb.

The model presented here naturally captures both driving forces. Indeed, the so-called 'global' emission model numerically represents f^{os}, while the 'local' model represents f^{el}. Fortunately, emission-dominated conditions lead to 'downward' climb, i.e. along the direction of the tensile region of the stress field of an edge dislocation, while absorption dominated climb takes place 'upwards', or towards the compressive semi-plane. As such, osmotic and stress-induced climb work in opposite directions, which allows us to separate their contribution.

Next, we apply the data in Fig. 5 (dashed lines) to eq. (20). The ratio of v_c and f^{os} gives the climb mobility, which we show in Fig. 7a as a function of inverse temperature and C_v.[5]

The results show that even after accounting for the linear temperature dependence of f^{os} (eq. (20)) M_c consistently displays an Arrhenius form of the type:

$$M_c(T, C_v) = A\left(\frac{C_v}{C_0}\right)\exp\left(-\frac{\Delta Q}{kT}\right) \tag{21}$$

where A is a pre-factor that depends on the C_v/C_0 ratio and ΔQ is an activation energy. The dependence of ΔQ on C_v is shown in the lower inset to Fig. 7a, where a weak decline from 1.7 to 1.2 eV can be appreciated. This correlates well with vacancy nucleation –characterized by an activation energy of 1.7 eV– playing a decreasingly important role as the global vacancy concentration increases. The dependence on the ratio $y = C_v/C_0$ is less clear (upper inset) but can be approximated reasonably well by a linear relation (shown as a dotted line on the upper figure inset):

$$A(y) = 1.9 \times 10^5 - 1.5 \times 10^3 y \quad [\text{Pa}^{-1}\ \text{s}^{-1}] \tag{22}$$

---

[4] Maintaining a constant vacancy supersaturation in globally acts as an inexhaustible vacancy source, with vacancies constantly being replenished as they disappear due to their interactions with dislocations.

[5] Note that no driving force exists when $C_v = C_0$ and so the climb velocity is nominally zero.
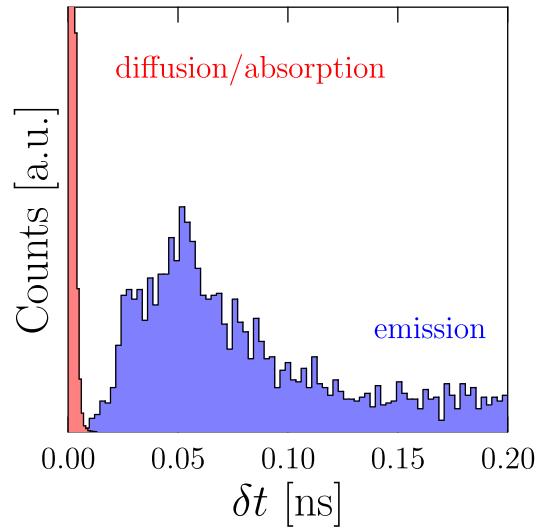
Fig. 6. Histogram of time steps in a general climb simulation at 1000 K. The red histogram (shorter timescales) represents the spectrum of δt associated with vacancy diffusion/absorption, while the blue one (longer time steps) represents vacancy emission events. The large spread in the distributions gives an idea of the range of stress spatial variations found in the computational domain. (For interpretation of the references to color in this figure legend, the reader is referred to the Web version of this article.)
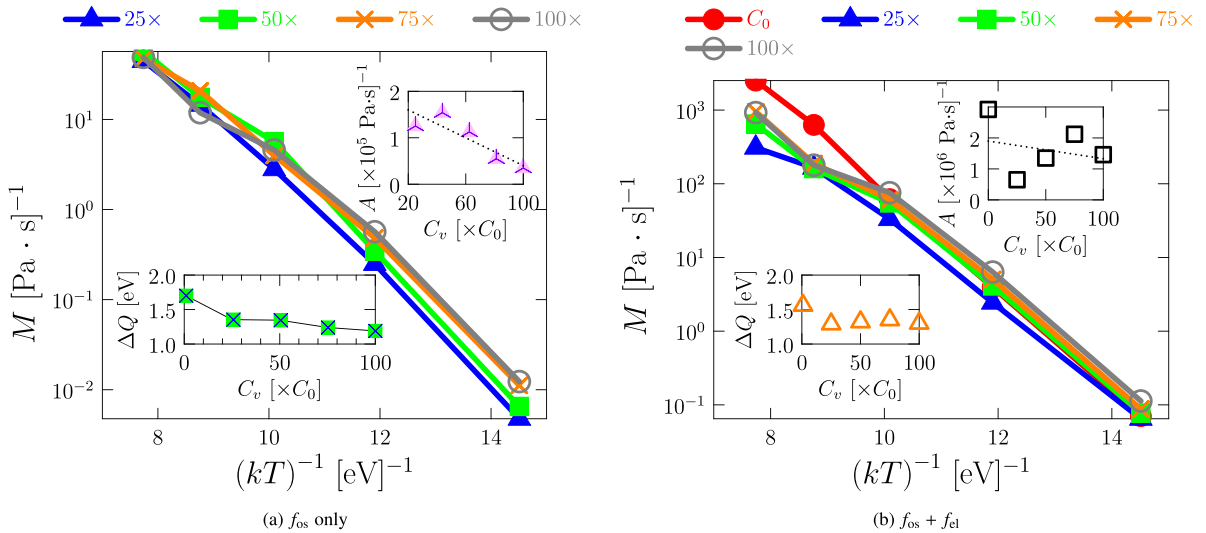
Fig. 7. Inverse temperature dependence of M_c for several nonequilibrium vacancy concentrations (given as a multiplier of the vacancy concentration $C_0(T, p)$). The lower and upper insets in both graphs show the activation energies and pre-factors for each curve, respectively, assuming an Arrhenius expression.

The above mobilities pertain to simulations under the action of chemical forces alone. When elastic forces act in conjunction with these chemical forces, we get the (negative) climb velocities given in Fig. 5. From these, as in eq. (21), a mobility can be extracted:

$$M_c = \frac{v_c}{f^{\text{el}} + f^{\text{os}}}$$

The only stress component conducive to climb is the diagonal component along the glide direction (i.e. $n \times t$, usually taken as σ_{xx}). However, while this component can be prescribed via the applied stress, local stresses due to jogs in the dislocation line can also contribute to the elastic climb force (recall Fig. 4). These are difficult to quantify, however, due to their highly local and fluctuative nature, which means that it is difficult to specify f^{el} with precision. If we go strictly by the applied force, the results of the analysis using the same tools as for eq. (20) are shown in Fig. 7b. As in Fig. 7a, the mobilities follow an Arrhenius evolution with temperature, characterized by the corresponding activation energies and pre-factors. The lower inset in Fig. 7b shows that the activation energies are

not unlike those for the case with no elastic forces, ranging between 1.5 and 1.3 eV. The pre-factors (upper inset in Fig. 7b), however, are approximately one order of magnitude higher than their 'chemical' counterparts. We attribute this difference to localized and fluctuating elastic climb forces that develop owing to the discrete nature of our model. These pre-factors do not exhibit a clear trend with C_v, showing almost a concentration-independent behavior:

$$A(y) = 1.9 \times 10^6 - 5.7 \times 10^3 y \quad [\text{Pa}^{-1} \text{ s}^{-1}] \tag{23}$$

Note that in the temperature range studied here, climb mobilities range from approximately three to four orders of magnitude smaller than glide mobilities at low temperatures, to comparable values at 1500 K (e.g., Gilbert et al. (2011); Queyreau et al. (2011)).

3.4. Application: dislocation climb over a spherical precipitate

We finish the Results section with a more practical application of the method. It is known that one of the mechanisms of dislocation-based creep is climb over precipitates that exert a force on dislocations greater than the glide force. Here, we simulate such a process by considering a spherical precipitate 4 nm in radius with an associated volumetric field characterized by stresses $\sigma_{rr} \propto 1/r^3$ (Ringdalen et al., 2017). The dislocation is then driven towards the precipitate by glide with a force insufficient to cut or loop around it. Aided by the volumetric force and by temperature, the dislocation can then climb by vacancy emission and circumvent the precipitate, continuing its glide. The simulations are conducted with a modified version of the DDLab code that includes spherical inclusions (Ringdalen et al., 2017) and to which we add the kMC module developed here. A sequence of snapshots showing this process, together with the number and position of the emitted vacancies is shown in Fig. 8. Note the relative large local concentration of vacancies along the climb path.

Additional analysis is given in Fig. 9 where the dislocation configuration at the point of maximum climb is provided. The color background in the figure represents the intensity of the radial stress caused by the precipitate in the matrix (in arbitrary units). The black dashed line represents the original glide plane (the equatorial plane of the precipitate), while the superimposed curve gives the number of vacancies emitted as a function of distance to the precipitate's outer radius. The combined action of the line tension, the glide force, and the precipitate stress field shape the dislocation line into an arced configuration as shown in the figure. Note that the timescale is arbitrary but the glide mobilities are about four orders of magnitude larger than climb mobilities.

These can be regarded as direct simulations of elementary creep mechanisms on time scales much longer than those associated with glide.

4. Discussion

4.1. The need for discreticity and stochasticity

First we justify the need for works such as the present one. Vacancy emission and diffusion are both thermally-activated processes, while dislocation network evolution is driven by elastic forces. However, while dislocation climb involves the conjunction of both phenomena, they typically act on very different length and time scales. Moreover, point defect processes are intrinsically stochastic in that they are driven by thermal fluctuations. As such, kMC is the pertinent method to study them, whereas DDD is the preferred tool to simulate dislocation dynamics. This work combines both techniques in a self-consistent way, i.e. (i) DDD resolves the elastic fields created by the dislocation structure, (ii) the kMC module evolves the vacancy subpopulation embedded in these fields, and (iii) dislocation-defect processes alter the dislocation substructures, giving rise to updated elastic fields. To our knowledge, the only prior work where kMC was linked to DDD is that by Ghoniem et al. (2002) to study defect decoration of dislocation loops. Our approach considers a drift on vacancy diffusion created by stress fields, which leads to an expression governed by stress gradients. This problem has been considered by several authors in the past (Bullough and Newman, 1970; Olmsted et al., 2004), albeit using a different approach to the one presented here.

Another thing worth emphasizing of this work is its discrete nature. Studies where the point nature of defects is directly accounted
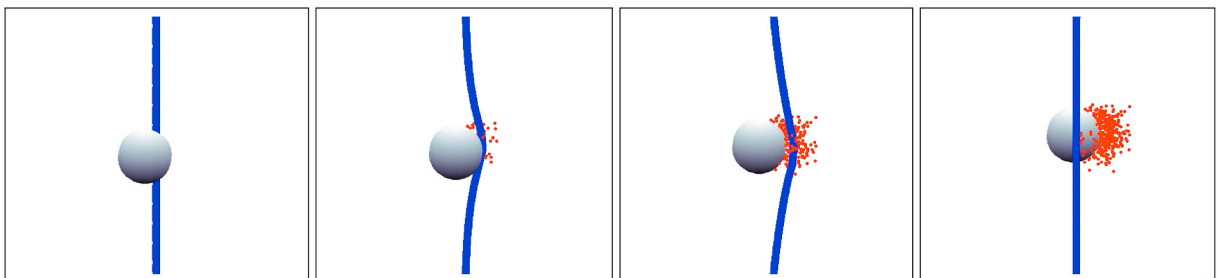
Fig. 8. Sequence of snapshots of an edge dislocation undergoing climb over a spherical precipitate in equilibrium conditions. The applied stress produces a force only along the glide direction that is insufficient to curve the dislocation around the precipitate on the glide plane. The images show the vacancies emitted while the dislocation climbs.
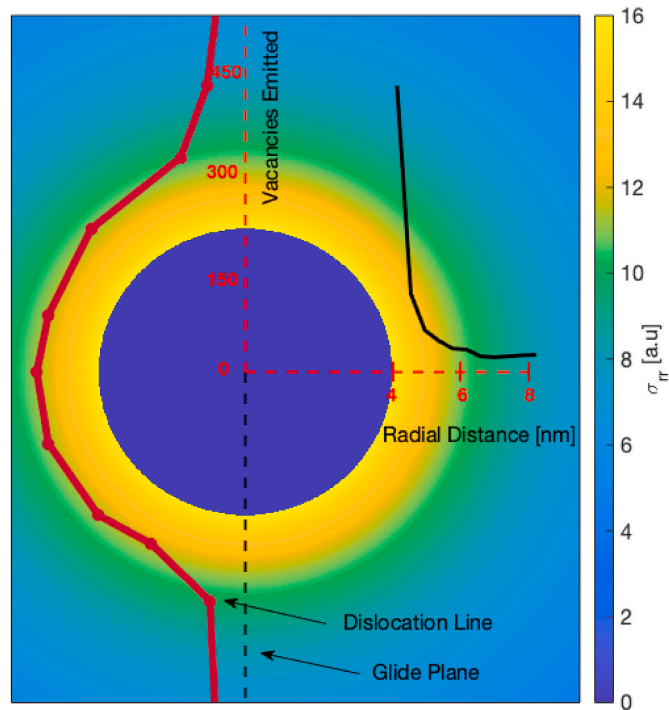
Fig. 9. Dislocation configuration at the point of maximum climb during simulations of temperature-enabled precipitate bypassing by an edge dislocation. The precipitate has spherical shape with a radius of 4 nm. The color background represents the intensity of the radial stress caused by the precipitate in the matrix (in arbitrary units). The black dashed line represents the original glide plane (the equatorial plane of the precipitate), while the superimposed curve gives the number of vacancies emitted as a function of distance to the precipitate's outer radius. (For interpretation of the references to color in this figure legend, the reader is referred to the Web version of this article.)

for are rare in the plasticity and DDD community. Direct atomistic calculations can only cover limited length and time scales (Nam and Srolovitz, 2007; Kabir et al., 2010), often too small or too short for steady state defect fluxes to occur. Mesoscopic models are better equipped to deal with the combination of small length scales and long time scales, but they can suffer from numerical stiffness. A model of dislocation climb based on elementary jog kinetics has been recently proposed (Niu et al., 2017). These are examples that discreticity and elasticity can be merged with relative high efficacy. Our method is a demonstration that defect generation, absorption, and diffusion can be treated in a point-like manner in conjunction with discrete dislocation dynamics.

It is important to note, however, that some relevant vacancy-related mechanisms are not captured by the present model. We do not consider pipe diffusion (diffusion along the dislocation line), which is known to be of importance in certain cases (Love, 1964; Mimkes, 1975; Miller et al., 1981; Gao et al., 2011). As well, vacancy clustering is not a feature of our approach, although atomistic studies have revealed conclusively that small vacancy clusters are unstable and have a short lifetime in bcc metals at the high temperatures explored here (Osetsky et al., 2000; Kiritani, 2000; Zinkle and Matsukawa, 2004). Finally, our results pertain to bulk material grains, without considering the effects of grain boundaries, which are known to be very effective vacancy sources/sinks and could alter the local and global vacancy supersaturation limits compared to those in ideal conditions.

4.2. Climb dynamics

Climb takes place under the action of two distinct forces, see eq. (19). The osmotic force is characterized by vacancy absorption due to the existence of a vacancy supersaturation and, as such, results in 'upwards' climb (along the direction of the compressive half-plane). Elastic climb, on the other hand, activates itself via vacancy emission and thus leads to climb in the direction of the tensile half-plane of the edge component of a dislocation. This elastic force clearly represents a mechanical bias conveyed by the stress at each point. The osmotic force, while in principle not a bias in the thermodynamic sense, is influenced by the stress gradient via the drift term in eq. (14), which can also be regarded a mechanical bias (although a second order one, see B). In this sense, our approach differs from the classical one in that locality is a feature of both f^{el} and f^{os}, not just of f^{el} (Lothe and Hirth, 1967; Turunen and Lindroos, 1973; Turunen, 1976; Raabe, 1998; Mordehai et al., 2008; Bakó et al., 2011).

Indeed, the classical treatment of dislocation climb suggests that the osmotic force scales with the vacancy supersaturation level. However, as our approach reveals, at the local level (near each dislocation segment), the local concentration is often zero, so that the driving force for vacancy emission is almost independent of the global vacancy concentration. As well, stress induced climb is seen to clearly dominate over chemical climb because the mechanical bias that controls vacancy emission (local stresses) is dominant over

drift effects brought about by stress gradients that control vacancy absorption.

4.3. Mobility functions

Mobility functions relate forces (stresses) and dislocation velocities and thus are an essential constitutive input to DDD simulations. For climb, it is generally impractical to simulate vacancy-dislocation coevolution in the manner done here, or as in molecular dynamics simulations. Hence, the present simulations should be seen as an intermediate step linking vacancy kinetics with dislocation dynamics, providing a general-purpose mobility functions with dependencies on the relevant state variables of the problem. Several authors have derived climb mobilities of the type (Turunen and Lindroos, 1973; Nix et al., 1971; Mordehai et al., 2008; Bakó et al., 2011): obtained by linearizing the exponential term containing the mechanical work done by the elastic force (D_v is the vacancy diffusivity, and r_∞ and r_0 are the standard elastic integration limits around a dislocation). θ represents the dislocation character, with $\sin\theta = 1$ for edge dislocations. The application of this expression in DDD simulations has been tested in depth (Zhuang et al., 2019) showing that it can work qualitatively for situations such as prismatic loop expansion and 'raft' microstructure formation. Our expression, by contrast, emanates from elementary vacancy processes such as lattice diffusion, emission, and absorption, and includes spatial and time fluctuations intrinsically. A comparison of both mobilities in the $800 < T < 1500$ K interval is provided in Fig. 10. An obvious difference is that, in our treatment, the mobility function itself depends on the vacancy supersaturation C_v/C_0, whereas eq. (24) does not. The most important difference to note, however, is how much faster the present mobilities are compared to the classical ones represented by eq. (24) (between two to three orders of magnitude, respectively, at high and low temperatures). We again rationalize this in terms of the local nature of vacancy absorption/emission, which is not captured by classical models based on homogeneous vacancy concentrations and smooth defect fluxes into or out of dislocation segments. Further studies are recommended to establish the correct time scale of climb in bcc metals.

$$M_c = \frac{2\pi D_v \Omega_a C_0}{kTb^2 \sin^2\theta \ln(r_\infty/r_0)} \tag{24}$$

The final expression for the climb velocity for general use in DDD simulations is:

$$v_c = A(y)\exp\left(-\frac{\Delta Q(y)}{kT}\right)\left[\frac{kT}{\Omega_a}\left(\frac{y-1}{y}\right) - \sigma_{xx}\right]b\sin\theta \tag{25}$$

where $y = \frac{C_0}{C_v}$, $\Delta Q(y) \approx 1.3$ eV and $A(y)$ given by eqs. (22) and (23), σ_{xx} is the corresponding component of the local stress tensor at segment i, $\boldsymbol{\sigma}(r_i)$, and $\theta = \cos^{-1}\left(\frac{\boldsymbol{b}\cdot\boldsymbol{t}}{b}\right)$.

5. Conclusions

We separate our conclusions into those relevant for the theory of plasticity and those that are technical in nature. Our main physical conclusions are:

- Stress gradients control vacancy diffusion in the presence of dislocation elastic fields. This results in a drift on vacancy transport that steers defects towards dislocation cores, conferring a mechanical bias to an otherwise 'chemical' process.
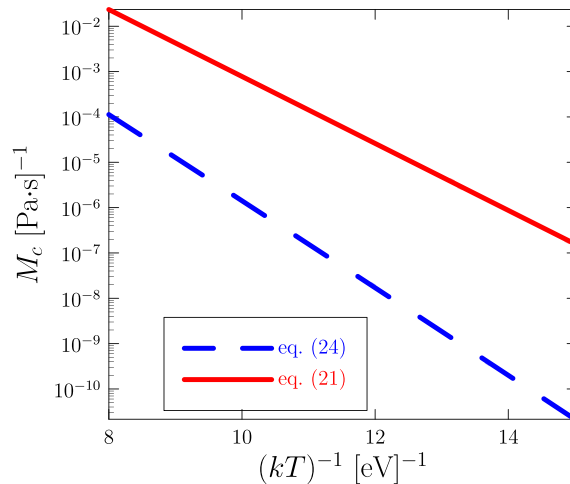
Fig. 10. Comparison between eq. (21) (present climb mobility expression, dashed blue) and (24) (expression by Bakó et al. (2011), red continuous). (For interpretation of the references to color in this figure legend, the reader is referred to the Web version of this article.)

- Climb is dominated by vacancy emission even when the background vacancy concentration is much higher than the equilibrium one. This is because local vacancy conditions control the overall kinetics, as captured in our approach, whereas classical treatments assume smooth vacancy fluxes from homogeneous defect concentrations.
- Climb velocities might be much faster than otherwise believed when one uses the classical theory of climb. Again, a consequence of local vacancy-dislocation interactions.

Our main technical conclusions are:

- We have developed a discrete stochastic model of vacancy evolution in the presence of arbitrary elastic fields furnished by DDD methods. Vacancy kinetics include emission, diffusion, and absorption, rigorously coupled to underlying dislocation fields, while absorption/emission events change the dislocation microstructure which is updated in time and, with it, the elastic fields.
- The method enables the calculation of dislocation climb mobility functions as a function of temperature, pressure, and vacancy concentration, to be directly used in parametric DDD simulations. The calculated climb mobilities are over $100 \times$ larger than those from previous derivations.
- Preliminary calculations of dislocation bypassing of spherical precipitates demonstrate that the method is capable of simulating physical processes conducive to high-temperature creep.

Declaration of competing interest

The authors declare that they have no known competing financial interests or personal relationships that could have appeared to influence the work reported in this paper.

Acknowledgement

Appendix A. Numerical solution procedure

The challenge in solving eq. (14) using expression (8) is that δx_i and u_i have an implicit relationship. That is, to compute u_i one needs to know δx_i, which itself is sampled from the solution to the drift-diffusion equation (8) which requires u_i as an input. Solving this requires running a self-consistent iterative procedure until the values of δx_i and u_i self-consistently converge.

Appendix A.1 The Box-Müller sampling

To sample from eq. (8) we use the Box-Müller approach (Golder and Settle, 1976), by which two random samplings z_1 and z_2 are generated using:

$$z_1 = \sqrt{-2 \ln \xi_1} \cos(2\pi\xi_2)$$

$$z_2 = \sqrt{-2 \ln \xi_1} \sin(2\pi\xi_2)$$

where ξ_1 and ξ_2 are two uniformly distributed random numbers in the (0, 1] interval. From this, the jump steps obtained are:

$$(\delta x_i)_{1,2} = u_i\delta t + z_{1,2}\sqrt{2D\delta t} \tag{A.1}$$

Note that δt is an input to the sampling procedure, but it is *a priori* unknown. This means that it also should be determined self-consistently (iteratively).

Appendix A.2. Numerical algorithm

Next, we present the recursive algorithm used to integrate the transport equations.

Algorithm 1. Numerical procedure to solve the vacancy elasto-diffusion model.

Algorithm 1 Numerical procedure to solve the vacancy elasto-diffusion model.

1: Initialize: TOL, `maxiter`, t_{TOT}.
2: **for** $n = 1$, `maxiter` **do**
3:     Initialize: $\delta t = \delta t^{n-1}$, $\delta t' = 0$.
4:     Initialize/update: R_{TOT}
5:     Initialize/update: $N, M \rightarrow$ DDD lib.
6:     **while** $|\delta t - \delta t'| > $ TOL **do**
7:         **for** $ivac = 1, N$ **do**
8:             Get: $\mathbb{R}^3$ point $\boldsymbol{P}(ivac)$
9:             Get: stress tensor $\boldsymbol{\sigma}(\boldsymbol{P}) \leftarrow$ DDD lib.
10:            Calculate: $\nabla_x \text{Tr}(\boldsymbol{\sigma})$ vector at $\boldsymbol{P}$ as indicated in eq. (14).
11:            **for** $j = 1, 3$ **do**
12:                Select: trial jump step δx_j.
13:                **while** $|\delta x_j - \delta x'_j| > $ TOL **do**
14:                    Calculate u_j from δx_j and $\partial \sigma_{kk}/\partial x_j$ using eq. (14).
15:                    Using u_j and δt, sample $\delta x'_j$ from Gaussian distribution (8).
16:                **end while**
17:                Calculate reaction rate: r_j^{ivac} as: $r_j^{ivac} = \left(2D/\delta x'_j\right)^2$
18:                $R_{TOT} = R_{TOT} + r_j^{ivac}$
19:            **end for**
20:        **end for**
21:        **for** $idisl = 1, M$ **do**
22:            Resolve all vacancy absorption instances and update nodal network (refer to eq. (15)) $\leftrightarrow$ DDD lib.
23:            Calculate vacancy emission rate r_{idisl} according to eq. (17).
24:            $R_{TOT} = R_{TOT} + r_{idisl}$
25:        **end for**
26:        Sample $\delta t'$ from Poisson distribution: $\delta t' = (R_{TOT})^{-1} \ln \chi$ (χ is a uniform random number).
27:    **end while**
28:    Sample event from uniform distribution R_{TOT} using binary search tree.
29:    Execute event: $\begin{cases} \text{- Displace vacancy along each directions by amount } \delta x_j, j = 1, 2, 3 \\ \text{or} \\ \text{- Insert vacancy in box} \end{cases}$
30:    $t_{TOT} = t_{TOT} + \delta t'$
31:    $n = n + 1$
32: **end for**

---

where N and M are, respectively, the number of vacancies and dislocation segments in the simulation box at any give time step. In this fashion, the DDD method acts as a library linked to the main workflow loop, from which information is passed bidirectionally. These links are highlighted in red color in the algorithm. Basically, Algorithm 1 consists of two `for` loops nested within a `do-while` loop. Each of the `for` loops is tasked with computing event rates due to vacancy diffusion (first loop) and vacancy emission (second loop), respectively. As such, one runs over all vacancies while the other runs over all dislocation segments. The `do-while` loop ensures the self-consistency of the $\delta x \equiv \delta x'$ condition.

Appendix A.3. Computational cost

To assess the computational cost of the simulations conducted here (which follow Algorithm 1), we calculate the ratio of CPU time to simulated (physical) time as a function of pressure, temperature, and vacancy concentration. We find that temperature is overwhelmingly the dominant parameter, with pressure and vacancy concentration having only a minor impact on CPU time. An example is shown in Fig. A.11, where the ratio of CPU time to simulated time for local and global vacancy emission implementations is given as a function of simulated temperature and pressure (with $C_v = C_0$). Temperature is seen to exponentially increase the CPU cost, while pressures up to ± 100 MPa have little to no effect on the computational efficiency. The local treatment of vacancy emission adds a cost factor of approximately $100 \times$ to the simulations compared to the global implementation. This approximately scales with the number of dislocation segments in the simulation box, so that a local treatment of emission incurs in an extra cost associated with a linear sweeping over all dislocation segments. This knowledge can guide further simulation campaigns when CPU time is of the essence.
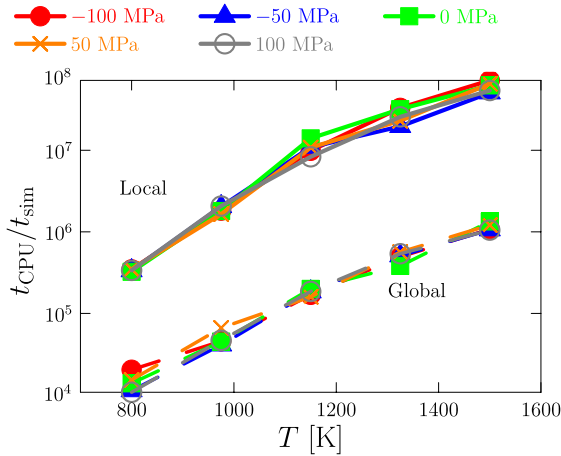
Fig. A.11. Ratio of CPU time to simulated time for local and global vacancy emission implementations as a function of simulated temperature and pressure (with $Cv = C_0$).

Appendix B. Second-order stress effects on the osmotic force

Starting from the general expression for the osmotic force in eq. (20):

$$f^{os} = \frac{bkT}{\Omega_a} \log \frac{C_v}{C_0} \tag{B.1}$$

one can refer C_v and C_0 to the *local* and *remote* concentrations near a dislocation core, such that the logarithmic term is expressed as $\log(C_{local}/C_{remote})$. This converts the spatial uniformity of C_v and C_0 to the level of proximity to a dislocation where stress gradients can be felt by vacancies.

C_{local} and C_{remote} can be replaced by their time dependent solutions (see eq. (8)):

$$C_{local}(x, t) = \frac{1}{(4\pi Dt)^{1/2}} \exp\left\{ -\frac{(x - ut)^2}{4Dt} \right\}$$

and

$$C_{remote}(x, t) = \frac{1}{(4\pi Dt)^{1/2}} \exp\left\{ -\frac{x^2}{4Dt} \right\}$$

Here we have assumed that vacancies near dislocations cores feel stress gradients and are subjected to a drift, while far away from them they do not. Inserting the above expressions into eq. (B.1) and operating:

$$f^{os} = \frac{bkT}{\Omega_a} \log \frac{C_{local}}{C_{remote}} = \frac{bkT}{\Omega_a} \log \frac{\exp\left\{ -\frac{(x-ut)^2}{4Dt} \right\}}{\exp\left\{ -\frac{x^2}{4Dt} \right\}} = \frac{bkT}{\Omega_a} \left[\frac{-(x - ut)^2 + x^2}{4Dt} \right] = \frac{bkT}{\Omega_a} \frac{ux}{2D} \tag{B.2}$$

where second order terms in time have been discarded. Replacing u by its expression in eq. (14), and assuming that $\|x\| \approx \delta x$:

$$u \approx \frac{D\Omega_a}{3kT} \nabla \text{Tr}(\boldsymbol{\sigma}) \tag{B.3}$$

leads to:

$$f^{os} \approx \frac{b^2}{3} \frac{\partial \sigma}{\partial x} \tag{B.4}$$

where it has been further assumed that the vacancy diffusion length is on the order of the Burgers vector's modulus.

Using the steady-state solution of the drift-diffusion equation leads to the same expression, assuming perfect vacancy absorbance at the dislocation core, and a uniform remote vacancy concentration of C_0, i.e. (Heald and Speight, 1975):

$$C^{\text{core}}(x) = C_0 \left(\frac{\exp\left\{\frac{ux}{D}\right\} - 1}{\exp\left\{\frac{u\ell}{D}\right\} - 1} \right)$$

Accordingly, the osmotic force becomes:

$$f^{\text{os}} = \frac{bkT}{\Omega_a}\left(1 - C^{\text{core}}/C_0\right) \approx \frac{bkT}{\Omega_{\text{rel}}} \left(\frac{\exp\left\{\frac{ux}{D}\right\} - 1}{\exp\left\{\frac{u\ell}{D}\right\} - 1} \right) = \frac{bkT}{\Omega_a} \left(1 - \frac{ux/D}{\exp\left\{\frac{u\ell}{D}\right\} - 1} \right) \tag{B.5}$$

where we have used a first-order expansion of the exponential, $x \equiv \delta x \approx 0$, and ℓ is a screening distance. This results in the expression:

$$f^{\text{os}} = \frac{bkT}{\Omega_a}\frac{u}{D}(\ell - \delta x) \tag{B.6}$$

which is identically equivalent to eq. (B.4) when $\delta x \approx b$ and $\ell \approx 2b$, both reasonable values for both parameters. This shows that when stress gradients are operative, the osmotic force is also subjected to a mechanical bias.

References

Arsenlis, Athanasios, Cai, Wei, Tang, Meijie, Rhee, Moono, Oppelstrup, Tomas, Hommes, Gregg, Pierce, Tom G., Bulatov, Vasily V., 2007. Enabling strain hardening simulations with dislocation dynamics. Model. Simulat. Mater. Sci. Eng. 15 (6), 553.

Bakó, Botond, Clouet, Emmanuel, Dupuy, Laurent M., Blétry, Marc, 2011. Dislocation dynamics simulations with climb: kinetics of dislocation loop coarsening controlled by bulk diffusion. Phil. Mag. 91 (23), 3173–3191.

Blaj, G., Kenney, C.J., Segal, J., Haller, G., 2017. Analytical Solutions of Transient Drift-diffusion in PN Junction Pixel Sensors arXiv preprint arXiv:1706.01429.

Bullough, R., Hayns, M.R., 1975. Irradiation-creep due to point defect absorption. J. Nucl. Mater. 57 (3), 348–352.

Bullough, R., Newman, R.C., 1970. The kinetics of migration of point defects to dislocations. Rep. Prog. Phys. 33 (1), 101.

Bullough, R., Quigley, T.M., 1981. Dislocation sink strengths for the rate theory of irradiation damage. J. Nucl. Mater. 104, 1397–1401.

Cai, Wei, Bulatov, Vasily V., 2004. Mobility laws in dislocation dynamics simulations. Mater. Sci. Eng., A 387, 277–281.

Codling, Edward A., Plank, Michael J., Benhamou, Simon, 2008. Random walk models in biology. J. R. Soc. Interface 5 (25), 813–834.

Davoudi, Kamyar M., Nicola, Lucia, Vlassak, Joost J., 2012. Dislocation climb in two-dimensional discrete dislocation dynamics. J. Appl. Phys. 111 (10), 103522. https://doi.org/10.1063/1.4718432.

Dederichs, P.H., Schroeder, K., 1978. Anisotropic diffusion in stress fields. Phys. Rev. B 17 (6), 2524.

Domain, C., Becquart, C.S., 2001. Ab initio calculations of defects in Fe and dilute Fe-Cu alloys. Phys. Rev. B 65 (2), 024103.

Dudarev, S.L., Mason, D.R., Tarleton, E., Ma, Pui-Wai, Sand, Andrea E., 2018. A multi-scale model for stresses, strains and swelling of reactor components under irradiation. Nucl. Fusion 58, 126002. https://doi.org/10.1088/1741-4326/aadb48.

Fischer, F.D., Svoboda, J., 2011. Chemically and mechanically driven creep due to generation and annihilation of vacancies with non-ideal sources and sinks. Int. J. Plast. 27 (9), 1384–1390.

Friedel, J., Yoshida, M., 1975. On dislocation jogs as sources and sinks of vacancies. Philos. Mag.: J. Theor. Exp. Appl. Phys. 31 (1), 229–231.

Fu, Chu Chun, Willaime, F., 2008. First principles calculations in iron: structure and mobility of defect clusters and defect complexes for kinetic modelling. Compt. Rendus Phys. 9 (3–4), 335–342.

Fu, Chu-Chun, Dalla Torre, Jacques, Willaime, François, Bocquet, Jean-Louis, Barbu, Alain, 2005. Multiscale modelling of defect kinetics in irradiated iron. Nat. Mater. 4 (1), 68.

Gao, Y., Zhuang, Z., Liu, Z.L., You, X.C., Zhao, X.C., Zhang, Z.H., 2011. Investigations of pipe-diffusion-based dislocation climb by discrete dislocation dynamics. Int. J. Plast. 27 (7), 1055–1071.

Ghoniem, N.M., Tong, S.H., Huang, J., Singh, B.N., Wen, M., 2002. Mechanisms of dislocation-defect interactions in irradiated metals investigated by computer simulations. J. Nucl. Mater. 307, 843–851.

Gilbert, M.R., Queyreau, S., Marian, J., 2011. Stress and temperature dependence of screw dislocation mobility in α-Fe by molecular dynamics. Phys. Rev. B 84 (17), 174103.

Golder, E.R., Settle, J.G., 1976. The box-Müller method for generating pseudo-random normal deviates. J. Roy. Stat. Soc.: Series C (Applied Statistics) 25 (1), 12–20.

Gu, Yejun, Xiang, Yang, Sin Quek, Siu, Srolovitz, David J., 2015. Three-dimensional formulation of dislocation climb. J. Mech. Phys. Solid. 83, 319–337.

Haghighat, SM Hafez, Eggeler, G., Raabe, Dierk, 2013. Effect of climb on dislocation mechanisms and creep rates in γ?-strengthened Ni base superalloy single crystals: a discrete dislocation dynamics study. Acta Mater. 61 (10), 3709–3723.

Heald, P.T., Speight, M.V., 1975. Point defect behaviour in irradiated materials. Acta Metall. 23 (11), 1389–1399.

Hertz, W., Waidelich, W., Peisl, H., 1973. Lattice contraction due to quenching in vacancies in platinum and gold. Phys. Lett. 43, 289–290.

Hirth, J.P., Lothe, J., 1992. Theory of Dislocations. Krieger, Malabar, Florida.

Hong, Sun Ig, 1986. Influence of dynamic strain aging on the dislocation substructure in a uniaxial tension test. Mater. Sci. Eng. 79 (1), 1–7.

Johnson, R.A., 1964. Interstitials and vacancies in α iron. Phys. Rev. 134 (5A), A1329.

Kabir, Mukul, Lau, Timothy T., Rodney, David, Yip, Sidney, Van Vliet, Krystyn J., 2010. Predicting dislocation climb and creep from explicit atomistic details. Phys. Rev. Lett. 105 (9), 095501.

Keralavarma, Shyam M., Cagin, Tahir, Arsenlis, A., Amine Benzerga, A., 2012. Power-law creep from discrete dislocation dynamics. Phys. Rev. Lett. 109 (26), 265504.

Kim, S.M., Buyers, W.J.L., 1978. Vacancy formation energy in iron by positron annihilation. J. Phys. F Met. Phys. 8 (5), L103.

Kiritani, Michio, 2000. Similarity and difference between fcc, bcc and hcp metals from the view point of point defect cluster formation. J. Nucl. Mater. 276 (1–3), 41–49.

Kraftmakher, Y., 1998. Equilibrium vacancies and thermophysical properties of metals. Phys. Rep. 299, 79–188.

Laidler, Keith J., King, M Christine, 1983. Development of transition-state theory. J. Phys. Chem. 87 (15), 2657–2664.

Landau, L.D., Lifshits, E.M., 1970. Theory of Elasticity. Pergamon Press, Oxford, England.

Leibfried, G., Breuer, N., 1978. Point Defects in Metals I: Introduction to the Theory. Springer-Verlag, Berlin.

Liu, Fengxian, Cocks, Alan CF., Tarleton, Edmund, 2019. A new method to model dislocation self-climb dominated by core diffusion. J. Mech. Phys. Solid. 103783.

Lothe, Jens, Hirth, John P., 1967. Dislocation climb forces. J. Appl. Phys. 38 (2), 845–848.

Louchet, François, Viguier, Bernard, 2000. Ordinary dislocations in γ-TiAl: cusp unzipping, jog dragging and stress anomaly. Philos. Mag. A 80 (4), 765–779.

Love, G.R., 1964. Dislocation pipe diffusion. Acta Metall. 12 (6), 731–737.

Ma, Pui-Wai, Dudarev, S.L., 2019a. Effect of stress on vacancy formation and migration in body-centered-cubic metals. Phys. Rev. Mater. 3, 063601. https://link.aps.org/doi/10.1103/PhysRevMaterials.3.063601.

Ma, Pui-Wai, Dudarev, S.L., 2019b. Universality of point defect structure in body-centered cubic metals. Phys. Rev. Mater. 3, 013605. https://link.aps.org/doi/10.1103/PhysRevMaterials.3.013605.

Mansur, Louis Kenneth, 1979. Irradiation creep by climb-enabled glide of dislocations resulting from preferred absorption of point defects. Philos. Mag. A 39 (4), 497–506.

Marian, J., Wirth, B.D., Odette, G.R., Perlado, J.M., 2004a. Cu diffusion in α-Fe: determination of solute diffusivities using atomic-scale simulations. Comput. Mater. Sci. 31 (3–4), 347–367.

Marian, Jaime, Cai, Wei, Bulatov, Vasily V., 2004b. Dynamic transitions from smooth to rough to twinning in dislocation motion. Nat. Mater. 3 (3), 158.

Martínez, Enrique, Marian, Jaime, Kalos, Malvin H., Perlado, José Manuel, 2008. Synchronous parallel kinetic Monte Carlo for continuum diffusion-reaction systems. J. Comput. Phys. 227 (8), 3804–3823.

Mendelev, M.I., Han, S., Srolovitz, D.J., Ackland, G.J., Sun, D.Y., Asta, M., 2003. Development of new interatomic potentials appropriate for crystalline and liquid iron. Phil. Mag. 83 (35), 3977–3994.

Messerschmidt, U., 1970. A model of the temperature dependent part of stage I work-hardening due to jog-dragging (I). Phys. Status Solidi 41 (2), 549–563.

Miller, K.M., Ingle, K.W., Crocker, A.G., 1981. A computer simulation study of pipe diffusion in body centred cubic metals. Acta Metall. 29 (9), 1599–1606.

Mimkes, Jürgen, 1975. Pipe diffusion along isolated dislocations. Thin Solid Films 25 (1), 221–230.

Mohamed, Farghalli A., Langdon, Terence G., 1974. The transition from dislocation climb to viscous glide in creep of solid solution alloys. Acta Metall. 22 (6), 779–788.

Mordehai, Dan, Clouet, Emmanuel, Fivel, Marc, Verdier, Marc, 2008. Introducing dislocation climb by bulk diffusion in discrete dislocation dynamics. Phil. Mag. 88 (6), 899–925.

Nam, Ho-Seok, Srolovitz, David J., 2007. Molecular dynamics simulation of Ga penetration along grain boundaries in Al: a dislocation climb mechanism. Phys. Rev. Lett. 99 (2), 025501.

Niu, Xiaohua, Luo, Tao, Lu, Jianfeng, Xiang, Yang, 2017. Dislocation climb models from atomistic scheme to dislocation dynamics. J. Mech. Phys. Solid. 99, 242–258.

Nix, W.D., Gasca-Neri, R., Hirth, J.P., 1971. A contribution to the theory of dislocation climb. Philos. Mag.: J. Theor. Exp. Appl. Phys. 23 (186), 1339–1349.

Núñez, M., Vlachos, D.G., 2015. Steady state likelihood ratio sensitivity analysis for stiff kinetic Monte Carlo simulations. J. Chem. Phys. 142 (4), 044108.

Olmsted, David L., Phillips, Rob, Curtin, W.A., 2004. Modelling diffusion in crystals under high internal stress gradients. Model. Simulat. Mater. Sci. Eng. 12 (5), 781.

Osetsky, Yu N., Bacon, D.J., Serra, A., Singh, B.N., Golubov, S.I., 2000. Stability and mobility of defect clusters and dislocation loops in metals. J. Nucl. Mater. 276 (1–3), 65–77.

Puchala, B., Falk, M.L., Garikipati, K., 2008. Elastic effects on relaxation volume tensor calculations. Phys. Rev. B 77, 174116. https://journals.aps.org/prb/abstract/10.1103/PhysRevB.77.174116.

Queyreau, S., Marian, J., Gilbert, M.R., Wirth, B.D., 2011. Edge dislocation mobilities in bcc Fe obtained by molecular dynamics. Phys. Rev. B 84 (6), 064106.

Raabe, D., 1998. On the consideration of climb in discrete dislocation dynamics. Philos. Mag. A 77 (3), 751–759. https://doi.org/10.1080/01418619808224081.

Rajaguru, M., Keralavarma, S.M., 2018. A discrete dislocation dynamics model of creeping single crystals. Model. Simulat. Mater. Sci. Eng. 26 (3), 035007.

Ringdalen, Inga, Wenner, Sigurd, Friis, Jesper, Marian, Jaime, 2017. Dislocation dynamics study of precipitate hardening in Al–Mg–Si alloys with input from experimental characterization. MRS Commun. 7 (3), 626–633.

Rovelli, I., Dudarev, S.L., Sutton, A.P., 2017. Non-local model for diffusion-mediated dislocation climb and cavity growth. J. Mech. Phys. Solid. 103, 121–141.

Rovelli, I., Dudarev, S.L., Sutton, A.P., 2018. Statistical model for diffusion-mediated recovery of dislocation and point-defect microstructure. Phys. Rev. 98 (4), 043002.

Savara, Aditya, Sutton, Jonathan E., 2018. SQERT-T: alleviating kinetic Monte Carlo (KMC)-stiffness in transient KMC simulations. J. Phys. Condens. Matter 30 (29), 295901.

Sivak, A.B., Chernov, V.M., Romanov, V.A., Sivak, P.A., 2011. Kinetic Monte-Carlo simulation of self-point defect diffusion in dislocation elastic fields in bcc iron and vanadium. J. Nucl. Mater. 417 (1–3), 1067–1070.

Snyder, M.A., Chatterjee, A., Vlachos, D.G., 2005. Net-event kinetic Monte Carlo for overcoming stiffness in spatially homogeneous and distributed systems. Comput. Chem. Eng. 29 (4), 701–712.

Söderlind, Per, Yang, L.H., Moriarty, John A., Wills, J.M., 2000. First-principles formation energies of monovacancies in bcc transition metals. Phys. Rev. B 61 (4), 2579.

Souidi, Abdelkader, Becquart, Charlotte S., Domain, Christophe, Terentyev, Dmitry, Malerba, Lorenzo, Calder, A.F., Bacon, D.J., Stoller, R.E., Osetsky, Yu N., Hou, Marc, 2006. Dependence of radiation damage accumulation in iron on underlying models of displacement cascades and subsequent defect migration. J. Nucl. Mater. 355 (1–3), 89–103.

Stoller, R.E., 1990. Modeling dislocation evolution in irradiated alloys. Metall. Trans. A 21 (7), 1829–1837.

Strunk, H., Frydman, R., 1975. Jog dragging in edge dislocations with application to plastic deformation and internal friction. Mater. Sci. Eng. 18 (1), 143–148.

Stukowski, Alexander, Cereceda, David, Swinburne, Thomas D., Marian, Jaime, 2015. Thermally-activated non-Schmid glide of screw dislocations in W using atomistically-informed kinetic Monte Carlo simulations. Int. J. Plast. 65, 108–130.

Thompson, D.H., Tarleton, E., Roberts, S.G., Fitzgerald, S.P., 2018. Interstitial-mediated dislocation climb and the weakening of particle-reinforced alloys under irradiation. Phys. Rev. Mater. 2 (8), 080601.

Turunen, M.J., Lindroos, V.K., 1973. Edge dislocation velocity in stress-induced climb. Philos. Mag.: J. Theor. Exp. Appl. Phys. 27 (1), 81–86.

Turunen, M.J., 1976. A general equation of motion for dislocation climb. Acta Metall. 24 (5), 463–467.

Vineyard, George H., 1957. Frequency factors and isotope effects in solid state rate processes. J. Phys. Chem. Solid. 3 (1), 121–127.

Wang, Jian, Hoagland, Richard G., Misra, Amit, 2009. Room-temperature dislocation climb in metallic interfaces. Appl. Phys. Lett. 94 (13), 131910.

Weertman, Johannes, 1955. Theory of steady-state creep based on dislocation climb. J. Appl. Phys. 26 (10), 1213–1217.

Záležák, Tomáš, Svoboda, Jiří, Dlouhý, Antonín, 2017. High temperature dislocation processes in precipitation hardened crystals investigated by a 3D discrete dislocation dynamics. Int. J. Plast. 97, 1–23.

Zhuang, Zhuo, Liu, Zhanli, Cui, Yinan, 2019. Chapter 12-glide-climb coupling model and temperature effect on microscale crystal plasticity. In: Zhuang, Zhuo, Liu, Zhanli, Cui, Yinan (Eds.), Dislocation Mechanism-Based Crystal Plasticity. Academic Press, pp. 331–380. http://www.sciencedirect.com/science/article/pii/B97801281 45913000121.

Zinkle, Steven J., Matsukawa, Yoshi, 2004. Observation and analysis of defect cluster production and interactions with dislocations. J. Nucl. Mater. 329, 88–96.